ANNUAL PROGRESS SUMMARY

To: tecnicalreports@afosr.af.mil
Subject: Annual Progress Statement to Dr. Arje Nachman

Contract/Grant Title: Mathematical Modeling and Experimental Validation of Ultrafast Nonlinear Light-Matter Coupling Associated with Filamentation in Transparent Media
Contract/Grant #: FA9550-10-1-0561
Reporting Period: September 30, 2010 to September 29, 2011

Annual accomplishments (200 words max):

First year MURI project highlights include: first theoretical insight into the evolution of nonequilibrium anisotropic photoionized electron/ion distributions, derived from a full quantum Schrödinger simulation, to a plasma state; rigorous computationally-efficient quantum photoionization model; theoretical investigation and experimental realization of novel nonlinear conical beams; spatial, temporal and phase control of ultrashort intense pulses (transverse and temporal profiles) and mid-IR filament enhanced phase matching higher harmonic generation. At the mathematical level, a new nonlinear pde model (modified Kadomtsev – Petviashvili evolution equation) simultaneously captures two classical singularities (blow-up and shocks) and the first application of asymptotic methods to weakly nonlinear conical beams implemented. Active collaborative multidisciplinary projects include: an Arizona – Colorado joint work on studying a new paradigm that captures the highly nonlinear physics interactions in the core of a light filament, an Arizona – Central Florida extension of linear conical waves (Bessel beams, Airy beams) into the nonlinear regime, a theory/experiment collaboration on HHG in high pressure gas waveguides involving Colorado, Cornel and Arizona, simulation of nonlinear temporal, phase evolution of femtosecond USPs with Temple and personnel exchange (postdoc, graduate student) between Colorado School of Mines and CREOL. Experimental personnel exchange between Arizona and the AFRL TeraWatt facility is ongoing.

Archival publications (published) during reporting period:

I. Chremmos, P. Zhang, J. Prakash, N. Efremidis, D. N. Christodoulides, and Z. Chen, "Fourier-space generation of abruptly autofocusing beams and optical bottle beams", *Optics Letters*, **36**, 3675 (2011).

P. Zhang, Z. Zhang, J. Prakash, S. Huang, D. Hernandez, M. Salazar, D. N. Christodoulides, and Z. Chen, "Trapping and transporting aerosols with a single optical bottle beam generated by Moiré techniques", *Optics Letters*, vol. 36, pp. 1491 (2011).

K. Glasner, M. Kolesik, J. Moloney and A. Newell "Canonical and Singular Propagation of Ultrashort Pulses in a Nonlinear Medium", *International Journal of Optics*, **2012**, Article ID 868274 (2011)

P. Polynkin and J. Moloney, "Self-focusing of femtosecond diffraction-resistant vortex beams in water", *Optics Letters*, **36**, 3834 (2011)

P. Polynkin and J. Moloney, "Optical breakdown of air triggered by femtosecond laser filaments", *Applied Physics Letters*, accepted (2011)

P. Zhang, J. Prakash, Z. Zhang, M. Mills, N. Efremidis, D. Christodoulides, and Z. Chen, "Trapping and guiding micro-particles with morphing auto-focusing Airy beams", *Optics Letters*, **36**, 2883 (2011).

P. Polynkin, M. Kolesik, E. Wright, J. Moloney, "Experimental tests of the new paradigm for laser filamentation in gases", *Physical Review Letters*, **PRL 106**, 153902 (2011).

I. Kaminer, M. Segev, and D. N. Christodoulides, "Self-Accelerating Self-Trapped Optical Beams", *Physical Review Letters,* **PRL 106**, 213903 (2011).

I. Chremmos, N. K. Efremidis, and D. N. Christodoulides, "Pre-engineered abruptly autofocusing beams," *Optics Letters,* **36**, 1890 (2011).

D. G. Papazoglou, N. K. Efremidis, D. N. Christodoulides, and S. Tzortzakis, "Observation of abruptly autofocusing waves," *Optics Letters*, **36**, 1842 (2011).

N. K. Efremidis and D. N. Christodoulides, "Abruptly autofocusing waves," *Optics Letters*, **35**, 4045 (2010).

W. Chong. H. Renninger, D. N. Christodoulides, and F. W. Wise, "Versatile Airy-Bessel light bullets", *Optics and Photonics News*, **December issue**, Optics in 2010, 52 (2010).

Changes in research objectives, if any: None

Changes in AFOSR program manager, if any: None

Extensions granted or milestones slipped, if any: None

Include any new discoveries, inventions or patent disclosures during this reporting period (if none, report none):

University of Arizona, Internal technical Disclosure UA12-030, “Remote Generation of Dense Plasma Channels Using Pulsed Lasers” (P. Polynkin, J.V Moloney)

Supplemental Material

Appended to this report are short technical reports from team members active within the MURI lead institute, University of Arizona and from all 5 external members of the MURI team. An important vehicle for more regular interaction and reporting amongst the MURI team members has been the semi-annual workshop held at the University of Arizona in March this year and a series of monthly telecons with each MURI team member.

Nonequilibrium electron plasma: isotropization/relaxation and coupling to THz fields

B. Pasenow,[1,2] J.V. Moloney,[1,2] M. Brio,[1] and S.W. Koch[2,3]

[1] *Arizona Center for Mathematical Sciences, Department of Mathematics, University of Arizona, Tucson, Arizona 85721*

[2] *College of Optical Sciences, University of Arizona, Tucson, Arizona 85721*

[3] *Department of Physics and Material Sciences Center, Philipps-University, 35032 Marburg, Germany*

(Dated: September 22, 2011)

COLLABORATIONS

Input for our work has been provided by S.H. Chen, A. Becker and A. Jaroń-Becker, *Ultrafast AMO Theory Group*, JILA and Department of Physics, University of Colorado at Boulder. Performing rigorous quantum calculations of the femtosecond ionization of hydrogen atoms in air they provide us with highly anisotropic electron and ion angular (momentum) distributions which serve as initial states for our investigations on the equilibration/isotropization dynamics. Chen et al. determine the initial momentum distribution of the electrons following strong field photoionization by solving the time-dependent Schrödinger equation of an individual hydrogen atom assuming an exciting linearly in z-direction polarized laser pulse. An example of such a distribution is shown in Fig. 1 (a). So far, the collaboration has led to a paper submitted to Physical Review Letters (see: STATUS PUBLICATIONS).

PROJECT DESCRIPTION

Based on fundamental quantum mechanical principles, it is clear that the development of a collective plasma state from initially uncorrelated electrons takes a finite time. Ultra short pulse (UPS) ionization of atoms and/or molecules initially generates a nonequilibrium distribution of electrons and ions. The quantum calculations by our collaboration partners from the University of Colorado show in particular the highly anisotropic nature of the USP generated electron distributions. Hence, these electrons are not in a plasma state which would be characterized by isotropic quantities like the plasma density, temperature and frequency.

Despite these facts, filamentation investigations [1, 2] often assume instantaneous, isotropic, plasma like (e.g. Drude model) properties of the photogenerated electrons. Clearly, such models ignore all nonequilibrium effects and make it impossible to describe e.g. the polarization dependence of the ultrafast optical response.

In recent times, there has been a flurry of activity and controversy concerning the nature and interpretation of the physics of USP strong field ionization and its interaction with a secondary probe [3–5]. In this context, our initial research interest is to analyze the nonequilibrium electron dynamics and to study how a common (isotropic) plasma state is established from an initially highly anisotropic state. In order to allow for experimental tests, we develop a theory for the THz response of the UPS generated electron/ion system. In particular, we show how the ionization induced anisotropy shows up in optical and THz pump probe experiments.

MICROSCOPIC PLASMA THEORY

For our investigations we apply a microscopic theory based on the formalism of the 2nd quantization where the equations of motion for the expectation value of an operator $\langle A\rangle$ is derived by solving the Heisenberg equation $-i\partial_t\langle A\rangle = \langle[H,A]\rangle = \langle HA - AH\rangle$. The Hamilton operator H includes the kinetic part, i.e. the free electron dispersion

$$H^{\lambda}_{kin} = \sum_{\lambda,\mathbf{k}} E^{\lambda}_{\mathbf{k}} \mathrm{a}^{+}_{\lambda\mathbf{k}} \mathrm{a}_{\lambda\mathbf{k}} \qquad \text{with } E^{\lambda}_{\mathbf{k}} = \frac{\hbar^2 k^2}{2m_\lambda}\,, \tag{1}$$

the many-body Coulomb interaction between charged electrons and ions ($\lambda,\rho \in \{e,i\}$)

$$H_C = \tfrac{1}{2} \sum_{\mathbf{k},\mathbf{p},\mathbf{q}\neq\mathbf{0}} \tfrac{q_\lambda}{q_\rho} \mathrm{V}^{\lambda\rho}_{|\mathbf{q}|} \mathrm{a}^{+}_{\lambda\mathbf{k}-\mathbf{q}} \mathrm{a}^{+}_{\rho\mathbf{p}+\mathbf{q}} \mathrm{a}_{\rho\mathbf{p}} \mathrm{a}_{\lambda\mathbf{k}} \qquad \text{with } \mathrm{V}_{|\mathbf{q}|} = \frac{1}{L^3} \frac{q_e^2}{\epsilon_0 (q^2+\kappa^2)} \tag{2}$$

and the interaction with a classical THz field

$$H^{\lambda}_{THz} = -\sum_{\lambda,\mathbf{k}} [\mathbf{J}^{\lambda}_{\mathbf{k}} + \tfrac{1}{2}\mathbf{J}^{\lambda}_{\mathbf{pond.}}] \cdot \mathbf{A}(t) \mathrm{a}^{+}_{\lambda\mathbf{k}} \mathrm{a}_{\lambda\mathbf{k}} \qquad \text{with } \mathbf{J}^{\lambda}_{\mathbf{k}} = \tfrac{q_\lambda}{m_\lambda}\hbar\mathbf{k} \text{ and } \mathbf{J}^{\lambda}_{\mathbf{pond.}} = -\tfrac{q_\lambda}{m_\lambda} q_\lambda \mathbf{A}(t) \tag{3}$$

where the light matter interaction is treated in the minimal coupling approach $\mathbf{p} \to \hbar\mathbf{k} - q_\lambda \mathbf{A}$. Here, $\mathbf{J}^{\lambda}_{\mathbf{pond.}}$ stands for the pondermotive contributions. The operator $\mathrm{a}^{+}_{\lambda\mathbf{k}}$ ($\mathrm{a}_{\lambda\mathbf{k}}$) creates (destroys) an electron ($\lambda = e$) or ion ($\lambda = i$) with momentum $\mathbf{k}$. Due to the large mass difference $m_e \ll m_i$ the ion energy can be usually neglected in comparison to the electron energy. The same holds for the ion current matrix element in eq. (3). Furthermore, for our ionization conditions the electron distributions $\mathrm{f}^{e}_{\mathbf{k}} = \langle \mathrm{a}^{+}_{e\mathbf{k}} \mathrm{a}_{e\mathbf{k}} \rangle$ can be treated in the non-degenerate limit, i.e. $(1 - \mathrm{f}^{e}_{\mathbf{k}}) \simeq 1$. These approximations/assumptions are used for the equations of motion of the following sections.

To investigate the ionization process and the evolution from the individual electron distribution into a collective plasma state, we have to solve the nonlinear light-matter interaction and the many-body dynamics governed by the electron-light, electron-electron and electron-ion Coulomb interactions. Ideally, one would have to treat the full problem of strong-field ionization together with the many-body dynamics at the level of quantum kinetic theory. However, for realistic systems, the numerical solution of the complete process is not feasible with current-day computer resources.

Fortunately, for the case of USP ionized electrons in dilute gases, the full problem can be simplified considering the basic physical conditions. The ionization with the high intensity light pulses happens on the timescale of several femtoseconds whereas for typical electron densities around $10^{23}/m^3$ the characteristic interaction time estimated from the inverse plasma frequency is in the picosecond range. This allows for the separation of the ionization and relaxation dynamics. Furthermore, a typical length scale for electrons should be around the Bohr radius ($a_B \simeq 0.05\,nm$) whereas the typical laser wavelengths (several 100 nm) or filament diameters (around $50\,\mu m$) are much larger. Therefore, we can restrict the electron dynamics after the ionization to an evolution of a quasi-homogeneous electron gas on the electronic length scale.

For our model investigations we treat a dilute gas of hydrogen atoms interacting with an intense short laser pulse. It has been shown [6] that momentum distributions obtained for the hydrogen atom are in quite good agreement with experimental data for noble gas atoms [7]. Nevertheless, these investigations can be considered as a first step which will be extended later in this project to treat also noble gases and molecules.

Delayed plasma state formation

For the relaxation dynamics of the anisotropic electron momentum distributions and the process of quasi-equilibrium plasma formation, the relevant equation is the quantum Boltzmann equation (BME) which includes drift and diffusion terms, the interaction with external fields and collision integrals. Since the electron-ion recombination happens on a nanosecond [8] timescale, the number of free electrons and ions is approximately conserved during the carrier relaxation into the quasi-equilibrium collective plasma state. Thus in the absence of further external fields, the BME reduces to its collision integrals,

$$\begin{aligned} \partial_t f^{e}_{k}|_{col} = {} & \frac{2\pi}{\hbar} \sum_{\mathbf{p},\mathbf{q}} V^2_{|\mathbf{q}|} (1 - f^{e}_{\mathbf{k}})(1 - f^{\lambda}_{\mathbf{p}}) f^{e}_{\mathbf{k}-\mathbf{q}} f^{\lambda}_{\mathbf{p}+\mathbf{q}} \delta(\Delta E^{e,\lambda}_{\mathbf{k},\mathbf{p},\mathbf{q}}) \\ & - \frac{2\pi}{\hbar} \sum_{\mathbf{p},\mathbf{q}} V^2_{|\mathbf{q}|} f^{e}_{\mathbf{k}} f^{\lambda}_{\mathbf{p}} (1 - f^{e}_{\mathbf{k}-\mathbf{q}})(1 - f^{\lambda}_{\mathbf{p}+\mathbf{q}}) \delta(\Delta E^{e,\lambda}_{\mathbf{k},\mathbf{p},\mathbf{q}}) \qquad \lambda \in \{e, i\}, \Delta E^{e,\lambda}_{\mathbf{k},\mathbf{p},\mathbf{q}} = \tfrac{\hbar^2|\mathbf{k}|^2 - \hbar^2|\mathbf{k}-\mathbf{q}|^2}{2m_e} + \tfrac{\hbar^2|\mathbf{p}|^2 - \hbar^2|\mathbf{p}+\mathbf{q}|^2}{2m_\lambda} \end{aligned} \tag{4}$$

where $f^{\lambda}_{\mathbf{k}}$ and m_λ denote the momentum dependent probability distribution and mass of the electrons ($\lambda = e$) and ions ($\lambda = i$), respectively. The δ-distribution $\delta(E)$ provides the energy conservation during the scattering.

The Coulomb potential $V_{\mathbf{q}}$ is screened using a Debye screening constant κ which is obtained as the $q = 0$-limit of the static Lindhard formula [9]. Due to their large mass, the ions hardly contribute to the screening and the electron-ion interaction is restricted to elastic scattering. This effectively decouples the electron from the ion dynamics since only the total ion density appears in the equation of motion for the electron distribution.

The Boltzmann collision integral conserves total momentum and energy, eventually describing the relaxation against a quasi-equilibrium Fermi-Dirac distribution. The moments of the distribution function therefore allow us to introduce a plasma density and temperature. In our approach, Eq. (4) is solved applying the Monte Carlo method. For our simulations we use up to 10^7 particles to describe the anisotropic distributions accurately. The Monte Carlo results

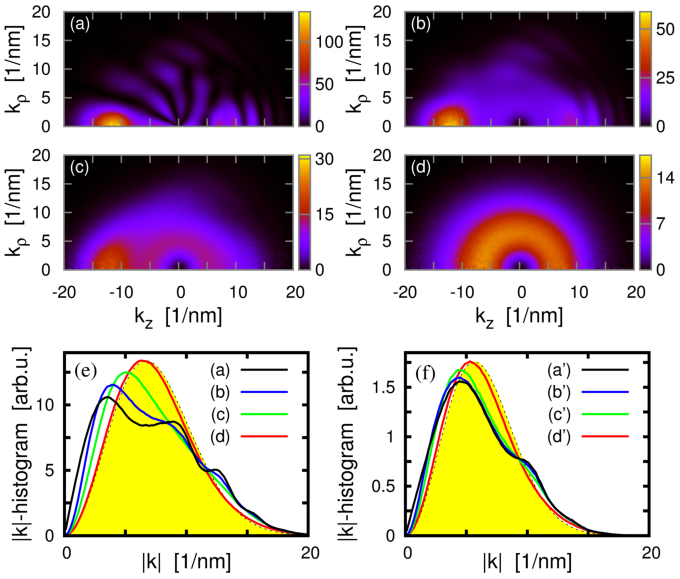

FIG. 1: Relaxation of an anisotropic nonequilibrium electron distribution created by ionizing hydrogen atoms with a $400\,nm$ 3-cycle pulse of intensity $I = 1 \times 10^{14} W/cm^2$ (a)-(e) or $I = 5 \times 10^{13} W/cm^2$ (f) respectively. Above, $H(k,\theta)$ for different times in units of $1/f_{pl}(N^e)$ (a) $t_0 = 0$, (b) $t_0 = 0.31$, (c) $t_0 = 1.04$ and (d) $t_0 = 6.25$. Here, $k_z = k\,cos(\theta)$ and $k_\rho = k\,sin(\theta) = (k_x^2 + k_y^2)^{1/2}$. Below, in (e) the corresponding θ-angle integrated $\bar{H}(k)$ and in (f) $\bar{H}(k)$ for the lower intensity at (a') $t_0 = 0$, (b') $t_0 = 0.31$, (c') $t_0 = 1.04$, (d') $t_0 = 6.27$. The yellow area shows the final Fermi Dirac distribution with $T = 19797\,K$ and $\bar{E} = 2.559\,eV$ for (e). The total electron density in (a)-(e) is $N^e = 2.155 \times 10^{23}/m^3$ which corresponds to an inverse 3D plasma frequency $1/f_{pl}(N^e) = 0.240\,ps$. The values for (f) are $T = 14273\,K$, $\bar{E} = 1.845\,eV$, $N^e = 2.402 \times 10^{22}/m^3$ and $1/f_{pl}(N^e) = 0.718\,ps$. *(taken from submitted PRL)*

are evaluated by calculating histograms from the ensemble of electrons $H(k,\theta) = \frac{k^2}{4\pi^2} f(k,\theta)$ and for comparison its θ-angle integrated version $\bar{H}(k) = \int sin(\theta) H(k,\theta)/2\,d\theta$. For an isotropic situation $H(k,\theta)$ will match $\bar{H}(k)$.

Fig. 1 shows a typical example of the numerically determined relaxation dynamics. The initially highly anisotropic distribution (a) becomes nearly isotropic on the timescale of an inverse plasma frequency (c) and equilibrates to a Fermi-Dirac distribution on a picosecond timescale (d). The anisotropy is here a measurement how far the state is removed from a common (isotropic) plasma state. As will be shown in the following it influences the THz answer to a weak probe pulse and makes it dependent on the polarization direction of the THz pulse, i.e. anisotropic.

Anisotropy in the linear response to a weak THz field

In order to investigate how the initially anisotropic electron distribution and its development into a collective plasma state could be tested experimentally, we calculate the response of the electron-ion system to a weak probe field with central frequency in the THz range of the electromagnetic spectrum. Here, we choose THz fields since typical UPS generated electron densities yield a plasma frequency in that range.

For these investigations we have to additionally include the light matter interaction with a THz field in our analysis. The derived equations are solved up to first order in the weak probe field (linear response theory) where the dynamics without probe corresponds to the theory presented in the previous section.

The equation of motion for the electron distribution $\mathrm{f}^e_{\mathbf{k}}$ does not couple directly to the THz field A(t).

$$\hbar\partial_t \mathrm{f}^e_{\mathbf{k}} = 2\sum_{\mathbf{q}} \frac{q_e}{q_i} \mathrm{V}^{ei}_{|\mathbf{k}-\mathbf{q}|} \mathrm{Im}\mathrm{C}^{ei}_{\mathbf{k},\mathbf{q}} + \hbar\partial_t \mathrm{f}^e_{\mathbf{k}}|_{ee\,scatter} + \hbar\partial_t \mathrm{f}^e_{\mathbf{k}}|_{ionization\,source} \tag{5}$$

A coupling is only possible via the electron-ion correlations $\mathrm{C}^{ei}_{\mathbf{k},\mathbf{q}}$.

$$-i\hbar\partial_t \mathrm{C}^{ei}_{\mathbf{k},\mathbf{q}} = \left[\mathrm{E}^e_{\mathbf{k}} - \mathrm{E}^e_{\mathbf{q}} + i\eta\right] \mathrm{C}^{ei}_{\mathbf{k},\mathbf{q}} - \mathbf{J}^e_{\mathbf{k}-\mathbf{q}} \cdot \mathbf{A}(t) \mathrm{C}^{ei}_{\mathbf{k},\mathbf{q}} + \frac{q_e}{q_i} \mathrm{V}^{ei}_{|\mathbf{k}-\mathbf{q}|} \left(\mathrm{f}^e_{\mathbf{q}} - \mathrm{f}^e_{\mathbf{k}}\right) L^3 N^i_{tot} \tag{6}$$

In Eq. (5), we formally added the electron-electron scattering contributions and the ionization part for which we use the results of the previous section. The coupled system of equations (5) and (6) is solved in frequency space which leads to an integral equation with a structure of Fredholm integral equation of type II.

For our investigations we assume ultrashort THz pulses centered at times t_0 which allow us to directly probe the distributions snapshots of Fig. 1 (a)-(d). Once we know the changes of the electron distribution induced by the THz field, the THz current can be calculated. It has two components, a potentially anisotropic non-pondermotive part from Eq. (5) and (6) which is sensitive to the full momentum distributions and an isotropic pondermotive part which

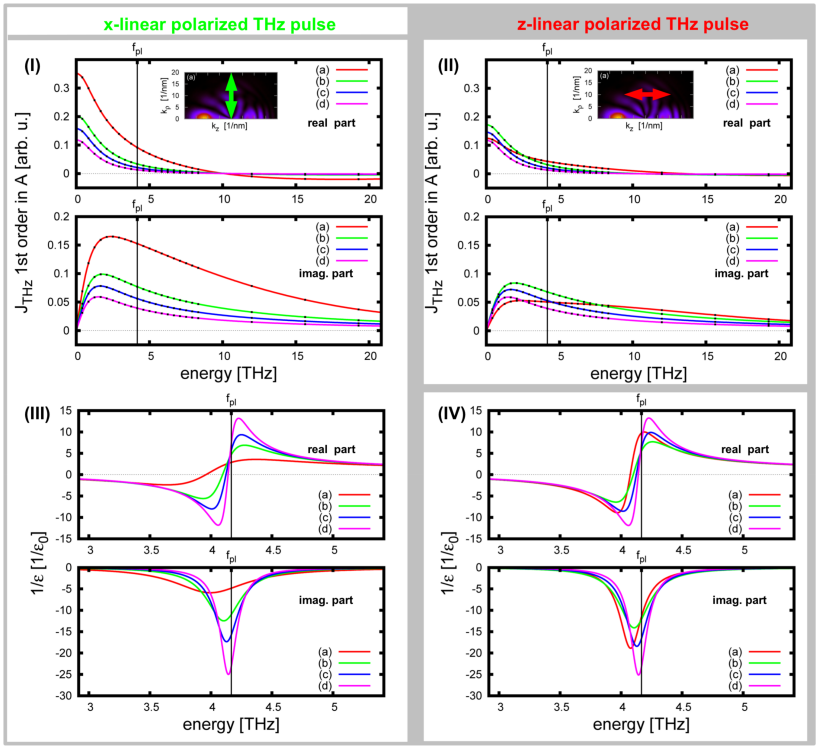

FIG. 2: Linear response to a weak THz pulse for a x-linear (I, III) and z-linear (II, IV) polarized THz pulse. Figure (I) and (II) show the THz induced non-pondermotive current calculated by solving eq. (5) and (6) up to linear order in the THz pulse. Figure (III) and (IV) show the corresponding inverse dielectric function (8). The colored lines (a)-(d) correspond to the distributions snapshots Fig. 1 (a)-(d). In the (nearly) isotropic case magenta line (d) no direction dependence remains.
(unpublished)

only depends on the total electron density

$$\mathbf{J}^{\lambda}_{\text{non pond.}} = \sum_{\lambda,\mathbf{k}} \mathbf{J}^{\lambda}_{\mathbf{k}}\, \mathrm{f}^{\lambda}_{\mathbf{k}} \qquad \text{with } \mathbf{J}^{\lambda}_{\mathbf{k}} = \tfrac{q_\lambda}{m_\lambda}\hbar\mathbf{k} \text{ and } \lambda \in \{e, i\}$$

$$\mathbf{J}^{\lambda}_{\text{pond}} = -\epsilon_0(\omega^{\lambda}_{pl})^2\mathbf{A}(\omega) \qquad \text{with } \omega^{\lambda}_{pl} = \sqrt{\frac{e^2 N^{\lambda}_{tot}}{m_\lambda \epsilon_0}} \tag{7}$$

With the current the linear susceptibility and therefore also the low frequency dielectric function can be defined

$$\chi(\omega) = \frac{J(\omega)}{\epsilon_0\omega^2 A(\omega)}, \qquad \epsilon(\omega) = \epsilon_b\left(1 - \frac{\omega^2_{pl}}{\omega^2}\right) + \frac{J_{THz}(\omega)}{\epsilon_0\omega^2 A(\omega)} \tag{8}$$

We solve these equations for two polarization directions, linear z-polarized which is also the polarization direction of the ionizing pulse and linear x-polarized. The results for the distributions Fig. 1 (a)-(d) are presented in Fig. 2. Here, we show the non-pondermotive current and the inverse dielectric function. The comparison of Figs. 2 (I) and (III) with (II) and (IV) demonstrates the polarization dependence of the THz response which gradually decreases during the isotropization of the distributions. The anisotropy of the distributions leads to an anisotropic THz answer. The imaginary part of the inverse dielectric function shows a resonance near the plasma frequency which might be used for measuring the plasma density in experiments.

SUMMARY

Our investigations clearly show that the high-intensity short-pulse ionization of atoms leads to highly anisotropic electron distributions. The quantum Boltzmann analysis allows us to identify two characteristic dynamical regimes during which the initial nonequilibrium distribution approaches a quasi-equilibrum plasma state. Due to the elastic and inelastic Coulomb scattering the electrons relax in a first step towards a hot nonequilibrium isotropic distribution. This is followed in a second step by a slower relaxation towards a Boltzmann distribution which is then indicative of a quasi-equilibrium, fully isotropic plasma state.

In order to suggest experimental verification of our predictions, we compute the response of the dynamical electron-ion system to a weak probe pulse in the THz regime of the electromagnetic spectrum. We find that the initially observed

strong polarization dependence of the THz response gradually relaxes as the isotropic plasma state is approached. Furthermore, we show how the THz response can be used to quantitatively measure the total density of ionized electrons.

STATUS PUBLICATIONS (09/23/2011)

submitted

B. Pasenow, J.V. Moloney, S.W. Koch, S.H. Chen, A. Becker, and A. Jaroń-Becker,
Nonequilibrium evolution of strong-field anisotropic ionized electrons towards a delayed plasma-state,
submitted to Phys. Rev. Lett. (2011)

in progress

B. Pasenow, J.V. Moloney, S.W. Koch, et al.,
topic: anisotropy in the linear THz response of a delayed plasma state

ACKNOWLEDGMENTS

We appreciate many stimulating discussions about the microscopic THz theory with M. Kira and D. Golde, University of Marburg, Germany. B. Pasenow thanks D. Vasileska, S.M. Goodnick and D.K. Ferry, Arizona State University, Phoenix (USA), for the very helpful introduction to the Monte Carlo method.

[1] M. Kolesik, J. V. Moloney, and M. Mlejnek, Phys. Rev. Lett. **89**, 283902 (2002).
[2] A. Couairon and A. Mysrowicz, Phys. Rep. **441**, 47 (2007).
[3] P. Béjot *et al.*, Phys. Rev. Lett. **104**, 103903 (2010).
[4] P. Polynkin, M. Kolesik, E. M. Wright, and J. V. Moloney, Phys. Rev. Lett. **106**, 153902 (2011).
[5] C. Brée, A. Demircan, and G Steinmeyer, Phys. Rev. Lett. **106**, 183902 (2011).
[6] D. Arbó *et al.*, Phys. Rev. Lett. **96**, 143003 (2006).
[7] A. Rudenko *et al.*, J. Phys. B: At. Mol. Opt. Phys. **37**, L407 (2004).
[8] Z. Sun, J. Chen, and W. Rudolph, Phys. Rev. E **83**, 046408 (2011).
[9] see, e.g. Chap. 8 in H. Haug and S.W. Koch, *Quantum Theory of the Optical and Electronic Properties of Semiconductors*, 5th edition, World Scientific Publ., Singapore (2009).

PDE Hierarchy for USP Filamentation

Patrick Whalen, Jerome V Moloney, Alan C Newell, Karl Glasner and Miroslav Kolesik

Department of Mathematics and College of Optical Sciences, University of Arizona

This project focuses on using asymptotic methods and direct derivations from vector Maxwell equations to establish a nonlinear pde hierarchy that describes different aspects of extreme NLO interactions associated with ultrashort pulse filamentation in gases and condensed media. Such nonlinear pdes provide the basis for analysis, isolate key nonlinear phenomena and provide for more efficient and coupling to new light-matter models being derived in parallel under this MURI program. By working in a spectral representation, we are able to seamlessly relate the workhorse UPPE propagator, other commonly employed nonlinear envelope propagators and our recent modified Kadomtsev-Petviashvilli model. The spectral form of UPPE, reduced to scalar form for simplicity is given by:

$$\partial_z E(k_\perp, z, \omega) = ik_z(\omega) E(k_\perp, z, \omega) + i\frac{\omega^2}{2\epsilon_0 c^2 k_z(k_\perp, \omega)} P_{NL}(k_\perp, z, \omega),$$

where, $E(k_\perp, z, \omega)$ represents the full electric field, the exact linear dispersion is contained in the z-component of the wavenumber and $P_{NL}(k_\perp, z, \omega)$ contains all nonlinear polarization sources.

By making the following envelope assumption

$$E(x_\perp, z, t) = A(x_\perp, z, t) e^{ik(\omega_R)z - i\omega_R t} + c.c.$$

Taylor expanding the exact linear dispersion relation about the reference wavenumber and frequency pair $(k_\perp, \omega)$ and retaining the leading order term in $k_\perp$ (paraxial approximation), we obtain the spectral representation of the NEE model due to Brabec and Krausz

$$\partial_z E(k_\perp, z, \omega) = -\frac{i}{2k(\omega_R)} \left(1 + \frac{\omega - \omega_R}{\omega_R}\right)^{-1} k_\perp^2 E + ik(\omega)E + \frac{ik(\omega_R)}{2\epsilon_0 n^2(\omega_R)} \left(1 + \frac{\omega - \omega_R}{\omega_R}\right) P_{NL}(k_\perp, z, \omega).$$

Alternatively, starting from UPPE above, but replacing the exact linear dispersion relation by the MKPI form

$$n_{MKP1}(\omega) = c\left(a\omega^2 - \frac{b}{\omega^2} + q\right).$$

and, assuming a paraxial approximation, the modified Kadomtsev-Petviashvilli equation follows

$$\partial_\tau\left(\partial_z E + \frac{4n_2}{c}E^2\partial_\tau E - a\partial_\tau^3 E\right) + bE = \frac{c}{2n(\omega_R)}\Delta_{(r)}E.$$

This pde model has been studied extensively in the literature (at least in 1D and 2D) and forms the basis for mathematical analysis. This pde model was also derived by us directly from the Maxwell equations using asymptotics. The asymptotic derivation relies on the following ordering of scales $z_{diffr}, z_{NL} << z_{Disp}$ where, z_{diffr} refers to the diffraction length, z_{NL} the nonlinear length and z_{Disp} the dispersion lengtn scale. Additionally, the MKPI model simultaneously captures two classical singularities namely, blow-up in finite time and carrier shocks.

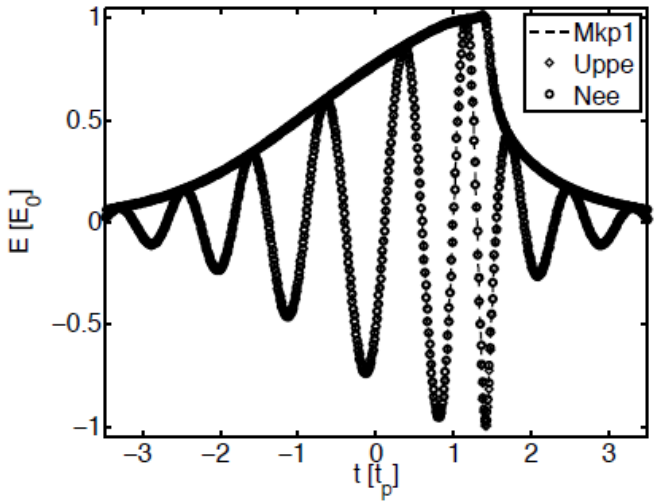

Figure 1 Carrier shock formation of a few-cycle USP

We currently comparing and contrasting UPPE, NEE and MKPI in order to establish physical parameter ranges where they become appropriate models of USP filamentation. A further goal is to couple these E.M propagators to more realistic but computationally feasible material models as they become available during the MURI project.

EXOTIC BEAMS WITH GAUSSIAN APODIZATION

Tobias Graf, Shankar Venkataramani

Arizona Center for Mathematical Sciences, Department of Mathematics, The University of Arizona, Tucson, AZ 85721-0089 USA

Asymptotic and Numerical Analysis of Conical Waves

We consider the effects of weak nonlinearities and Gaussian apodizations on the propagation behavior of conical waves, in particular Bessel-Gauss beams. These types of beams arise as nondiffracting solutions to the linear wave and Helmholtz equation (Lord Rayleigh 1897, Durnin 1987) as well as the paraxial wave or linear Schrödinger equation. We investigate the propagation behavior of conical waves with a Gaussian apodization under the cubic nonlinear Schrödinger equation (NLS) in one and two transverse dimensions. To do so, we use the same parameter to describe the aperture width the strength of the nonlinearity and treat the nonlinear problem as a perturbation of the ideal linear case. In this situation, we have developed a multiple scales method that allows us to derive amplitude equations from which we obtain interesting asymptotic solutions. Moreover, we have stated several uniform estimates that provide rigorous estimates for the approximation of an ideal Bessel beam. Furthermore, we are currently investigating numerically the applicability of the aforementioned amplitude equations for the numerical simulation of nonlinear conical waves with Gaussian apodizations. Preliminary experiments that compare the numerical solution of the amplitude equations to the result of a standard split-step Fourier method indicate that the amplitude equations yield a good approximation to the absolute value and real part of the solution even when evaluated on a much coarser transverse grid. The efficiency of a similar scheme in two transverse dimensions depends on the possibility of introducing symmetry assumptions to reduce the number of wave vectors for the amplitude equations have to be solved explicitly. This is currently work in progress.

In the case of two transvers dimension (1+2D), we consider the following cubic nonlinear Schrödinger (NLS) equation

$$-i\frac{\partial u}{\partial z}(x,y;z) = \Delta_{\perp}u(x,y;z) \pm \epsilon|u|\text{^}2u(x,y;z)$$

and initial conditions of the form

$$u(x,y;0) = \int_0^{2\pi} A_{\phi}\left(\frac{x}{N},\frac{y}{N}\right) e^{ia(x\cos\phi + y\ \sin\phi)} d\phi$$

where the initial amplitudes for a Bessel-Gauss beam of order n are given by

$$A_{\phi}\left(\frac{x}{N},\frac{y}{N}\right) = e^{-\left(\frac{x^2}{N^2}+\frac{y^2}{N^2}\right)} e^{in\phi}$$

for positive integers n. Note that an important difference to the case of one transverse dimension (1+1D) is the fact that the conical superposition in the 1+2D scenario consists in general of a continuous family of plane waves while we only have to consider finite sums when investigating conical waves in 1+1D.

For an analytical treatment of the initial value problem introduced above we assume that a solution can be developed in an asymptotic series of the for

$$u(x,y;z) = u_0(X,Y,Z_1,Z_2) + \frac{1}{N}u_1(X,Y,Z_1,Z_2) \; + \frac{1}{N^2}u_2(X,Y,Z_1,Z_2) + \cdots$$

where we introduce slowly varying amplitudes and put

$$u_0(x,y;z) = \int_0^{2\pi} A_\phi\,(X,Y,Z_1,Z_2,\ldots)e^{ia(x\cos\phi + y\,\sin\phi)}d\phi\; e^{-ia^2z}$$

in the above. We define the slow variables $X = \frac{x}{N}$, $Y = \frac{y}{N}$, $Z_1 = \frac{2az}{N}$, and $Z_2 = \frac{z}{N^2}$.

From the above mentioned framework we assume that the nonlinearity is of order 1/N, and we obtain asymptotic solutions for which we can state various uniform estimates. In particular, we recover conical regions that are analogous to the cone and diamond shaped Bessel regions described for example by Durnin (1987) and McGloin and Dholakia (2005). The above analytical framework is an improvement of the original approach suggested in the spring of 2011. The modified framework avoids or clarifies some of the simplifying assumptions that were necessary previously. We hope to extend at least some of our earlier results to this more general situation in the future.

Currently, we are investigating the possibility of using the amplitude in numerical simulations, in particular, we hope to obtain good approximations to the solution obtained from a standard split-step Fourier method, even when solving the amplitude equations on a significantly coarser grid. As mentioned previously, the search for symmetry reductions will be crucial for efficient numerical implementations.

At this time, we have submitted the following two papers for publication:

- T. Graf, J.V. Moloney, and S.C. Venkataramani. Weakly Nonlinear Conical Waves with Gaussian Apodization*. Submitted*, 2011.
- T. Graf, J.V. Moloney, and S.C. Venkataramani. Weakly Nonlinear Conical Waves with Gaussian Apodization in Two Transverse Dimensions. *Submitted*, 2011.

Furthermore, we have started to apply our multiple scales framework to the analysis of superpositions of higher order Bessel-Gauss beams for beam design purposes in a collaborative effort with M. Mills and D. Christodoulides at the University of Central Florida, CREOL.

Paraxial Equations and Initial Conditions with Gaussian Apodizations

(with M. Mills and D. Christodoulides at the University of Central Florida)

During and following a visit to the University of Central Florida, T. Graf has developed a scheme to obtain analytical solutions of the paraxial wave equation that correspond to finite energy waves due to a Gaussian apodization. The immediate motivation and application for this method is a project on linear optical bullets in two spatial transverse dimensions with anomalous dispersion by M. Mills and D. Christodoulides at CREOL. This situation corresponds mathematically to a 1+3D paraxial wave equation, and the analytical framework has been generalized to the 1+nD case where n is a positive integer. In summary, we can obtain an analytic solution of the paraxial wave equation

$$-i\frac{\partial u}{\partial z}(x_1,\dots,x_n;z) = \Delta_\perp u(x_1,\dots,x_n;z)$$

for the initial conditions

$$u(x_1,..,x_n;0) = e^{-\left(\frac{x_1^2+\cdots+x_n^2}{w^2}\right)}A(x_1,..,x_n;0),$$

where $A(x_1,..,x_n;z)$ is a solution of the paraxial equation, without going through the analytically tedious process of taking Fourier transforms, solving an ODE problem, and using inverse Fourier transforms. In particular, we have found coordinate transformations of the form

$$\tilde{x}_j(x_1,..,x_n;z) = \frac{x_j}{w^2+4iz}, j = 1,\dots,n \text{ and } \tilde{z}\,(x_1,..,x_n;z) = \frac{i}{4(w^2+4iz)}$$

such that the product

$$v(x_1,..,x_n;z) = G(x_1,..,x_n;z)\,A(\tilde{x}_1,..,\tilde{x}_n;\tilde{z})$$

is a solution to the paraxial wave equation. Here the function $G(x_1,..,x_n;z)$ denotes the solution of the paraxial wave equation with only Gaussian initial conditions.

$$G(x_1,..,x_n;0) = e^{-\left(\frac{x_1^2+\cdots+x_n^2}{w^2}\right)}$$

A discussion of the above mentioned analytical framework for a 1+3 dimensional equation with applications to linear optical light bullets is included in the following manuscript that we hope to submit for publication soon.

- M. Mills, G. Siviloglou, D. Christodoulides, T. Graf, and J. Moloney. Optical bullets with Hydrogen-like symmetries. In preparation.

References

- J. Durnin. Exact solutions for nondiffracting beams. I. The scalar theory. *J. Opt. Soc. Am. A*, 4(4):651-654, Apr 1987.
- D. McGloin and K. Dholakia. Bessel beams: diffraction in a new light. *Contemporary Physics*, 46(1): 15-28, 2005.
- Lord Rayleigh. On the passage of electric waves through tubes, or the vibrations of dielectric cylinders. *Philosophical Magazine*, 43, 1897.

Technical Progress Report (2011)

Karl Glasner[1],
[1] Department of Mathematics, University of Arizona

September 20, 2011

This report summarizes progress on mathematical modeling and analysis of models of ultra short pulse propagation.

1 Simplified models and singular behavior of broadband pulses

Collaborators: Miroslav Kolesik, Jerome V. Moloney, Alan C. Newell

Publication(s): "Canonical and Singular Propagation of Ultrashort Pulses in a Nonlinear Medium," International Journal of Optics, vol. 2012, (2012).

The goal of this work was to obtain a simplified model of a weakly dispersive broadband pulse starting from first principles. The outcome was a version of the Kadomtsev – Petviashvili equation

$$\frac{\partial}{\partial \tau}\left(\frac{\partial E_0}{\partial z}+\frac{\partial E_0^3}{\partial \tau}-B\frac{\partial^3 E_0}{\partial \tau^3}-A\frac{\partial^2 E_0}{\partial \tau^2}\right)=D\Delta_\perp E_0.$$

Numerical experiments were conducted on typical (few cycle) broadband initial conditions. Two types of singular behavior were observed. For vanishing normal dispersion, the pulse develops a temporal shock. For small (but not necessarily vanishing) anomalous dispersion, the pulse generates a genuine blow up singularity. In the latter case, the singularity is self similar (like NLS blow up) but exhibits both axial and temporal compression.

Present work is being conducted to relate this simplified model to more elaborate descriptions of broadband pulses (e.g. Kolesik & Moloney, Phys. Rev. E. 70 (2004)). The exact nature of the compression singularities is also being explored.

2 Singularities in cylindrical vector beams

Collaborators: Jordan Allen-Flowers (UA Graduate Program in Applied Mathematics)

Publication(s): Nearly self-similar ring solutions in the nonlinear Schroedinger equation, *in preparation.*

The critical nonlinear Schroedinger equation is known to have ring-type blow up solutions (see Fibich, Gavish & Wang, Physica D 2005). We have discovered similar blow up profiles in the azimuthally polarized version

$$iu_t + \Delta_v u + |u|^2 u = 0, \Delta_v = u_{rr} + (1/r)u_r - (1/r^2)u.$$

Self similar blow up profiles are known to exist, but do not have finite Hamiltonian, and therefore do not entirely explain why numerical simulations with realistic initial data develop ring-type solutions. The resolution to this paradox is in recognizing that there is a family of ring solutions for supercritical ($d > 2$) dimension (Budd, SIAM J. Appl. Math., 2001). These can be used to build approximately self-similar blow-up ring solutions for both regular and azimuthally polarized NLS.

Ab-initio numerical simulations of laser-matter interaction

Agnieszka Jaroń-Becker and Andreas Becker (JILA, University of Colorado at Boulder)

Physical models of laser pulse filamentation in the air rely on parameterized formula for the nonlinear susceptibility (Kerr coefficients) and multiphoton ionization rates. The corresponding parameters are either extracted from the experiment or theoretical models, which approximately describe the laser-matter interaction, e.g. by tunneling ionization. In view of the goal of the MURI to replace qualitative propagation models by a sophisticated hierarchy of analytical and computational mathematical tools, which can quantitatively capture the filamentation process, we have developed a new ab-initio method to solve the time-dependent Schrodinger equation for the interaction of the laser pulse with individual atoms and molecules in the filament [1]. Our method is based on recent efforts in electronic structure and materials calculations to use so-called numerical basis sets as an alternative to the well-studied analytical basis sets, such as Slater-type [2], Gaussian [3] or B-spline functions [4]. Recent quantum chemical calculations indicate that numerical basis state methods offer advantages in terms of computational efficiency over the previously used methods [5,6]. Furthermore, it is rather straightforward to extend the present method from the atomic to other systems, such as diatomic molecules or even more complex target systems.

In our method we first numerically obtain finite-space energy eigenstates for an (single-active-electron) atom or molecule in a box [7,8]. This basis is then represented on a grid and the system is propagated under the influence of an intense laser pulse using the Crank-Nicolson method. We applied the method to the hydrogen atom and tested the convergence of the results over a large variety of laser parameters as well as compared the results to those obtained with other numerical approaches. Next, we implemented the numerical basis state method in a parallel processing code. Our tests show the encouraging result that the speed-up factor $S=T_1/T_p$, where T_1 and T_p are the computational times for a single and p processors, respectively, increases almost linearly and the parallel efficiency $E=T_1/(NT_p)$ reaches about 75-80% as the number of processors increases (see Figure 1).

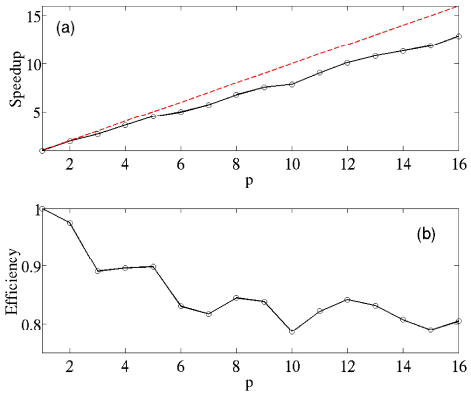

Figure 1: (a) Speedup factor and (b) parallel efficiency as a function of number of processors. Calculations were done for total excitation yield of the hydrogen atom in an ultrashort laser pulse of 2-cycles at 800 nm and a peak intensity of 1×10^{14} W/cm^2.

The new method is currently used in three projects within the MURI project:

(a) Laser pulses within laser pulse filaments often shorten to just a few-cycles in pulse durations. At these pulse lengths, the carrier-to-envelope phase (CEP) of the actual electric field oscillation to the amplitude envelope of the field becomes important [9]. We performed a systematic study of the CEP-effects on the excitation (and ionization) of the hydrogen atom. Our results (i) confirm recent theoretical predictions [10] of a strong dependence of the population in off-resonant energy levels on the CEP, (ii) provide new theoretical predictions for

the atomic excitation by pulses with steep envelopes at the front or the back of the pulse and (iii) provide a vivid explanation of the so-called frustrated ionization effect [11]. A manuscript covering the numerical basis-state method as well as the above mentioned applications is in preparation [1].

(b) In collaboration with the Arizona team (B. Pasenow, S.W. Koch, J.V. Moloney) we studied the evolution of highly anisotropic electron angular momentum distributions, generated during interaction of hydrogen atom with ultrashort laser pulses, into a nonequilibrium and then further into a quasi-equilibirum distribution [12]. To this end, we determined the initial electron momentum distributions following strong-field multiphoton ionization from the ground state of the hydrogen atom for various laser parameters.

(c) In collaboration with the CU Experiment team (M. Murnane, H. Kapteyn) we started to investigate strong-field ionization processes at different laser wavelengths, in particular, in the infrared regime beyond the Ti:Sapphire wavelength regime. We analyze how information about the attosecond electron dynamics in the atom and molecule as well as in the continuum is encoded in the electron momentum distributions. Examples for the results of our calculations are shown in Figure 2. Our findings will contribute to develop an advanced understanding of the recently introduced electron holography method [13].

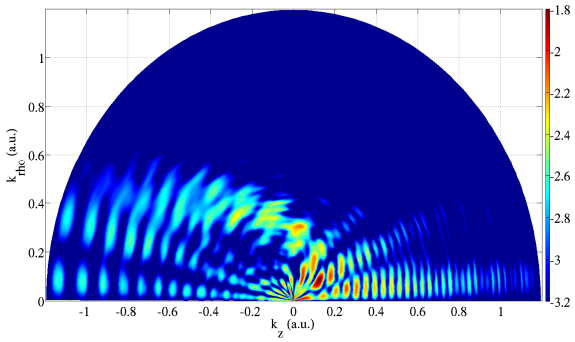

Figure 2: Electron momentum distribution following ionization of the hydrogen atom with a 3-cycle laser pulse at 1300 nm and a peak intensity of 2×10^{14} W/cm^2, the carrier-to-envelope phase is set to zero.

References:

[1] S.H. Chen et al., in preparation for submission to Phys. Rev. A
[2] E. Clementi and C. Roetti, At. Data Nucl. Data Tables **14**, 177 (1974).
[3] A. Szabo and N.S. Ostlund, *Modern Quantum Chemistry* (Dover Publications, 1996)
[4] H. Bachau et al., Rep. Prog. Phys. **64**, 1815 (2001)
[5] N.A. Benedek et al., J. Chem. Phys. **122**, 144102 (2005)
[6] D.J. Henry et al., J. Phys. Chem. **112**, 9835 (2008)
[7] S.H. Chen and J.M. Li, Chin. Phys. Lett. **23**, 2717 (2006)
[8] X. Gao et al., Chin. Phys. Lett., **26**, 013102 (2009)
[9] G.G. Paulus et al., Nature **414**, 182 (2001)
[10] T. Nakajima and S. Watanabe, Opt. Lett. **31**, 1920 (2006)
[11] T. Nubbemeyer et al., Phys. Rev. Lett. **101**, 233001 (2008)
[12] B. Pasenow et al., submitted for publication in Phys. Rev. Lett.
[13] Y. Huismans et al., Science **331**, 61 (2011)

People involved in the project:

Dr. Agnieszka Jaroń-Becker and Dr. Andreas Becker (Principal Investigators, not supported by the project)

Dr. Shaohao Chen (Postdoctoral researcher, supported by the project February – May 2011, now at Louisiana State University)

Andrew Spott (Graduate student, supported by the project since August 2011)

Papers submitted as result of the MURI project

- B. Pasenow, J.V. Moloney, S. W. Koch, S. H. Chen, A. Becker and A. Jaroń-Becker, *"Nonequilibrium evolution of strong-field anisotropic ionized electrons towards a delayed plasma state",* submitted to Physical Review Letters

Papers in preparation as result of the MURI project

- Shaohao Chen, Andrew Spott, Xiang Gao, Jiaming Li, Andreas Becker, and Agnieszka Jaroń-Becker, *"Application of numerical basis state method to strong-field excitation and ionization of hydrogen atom"***,** in preparation for submission to Physical Review A

Understanding Intense Laser Beam Filamentation in the Mid-IR region using Strong Field Ionization and Coherent X-Ray Generation as Probes

Margaret Murnane and Henry Kapteyn, JILA

In recent work, we demonstarted that by using mid-infrared lasers in the 1 – 4 μm region of the spectrum, it is possible to phase match the high-order harmonic generation (HHG) process at photon energies > 1 keV.[1-3] Fortunately, the conditions required for phase matching coincide closely with the ultrashort-pulse filamentation regime of interest for directed energy applications.[4] As well as utilizing driving lasers in the mid-infrared eyesafe region of the spectrum, the required pulse energies are in the millijoule range, fractional ionization of the plasma is in the range of 1%-0.001%, the optimal gas pressures are in the range of 1-10 atm, *and the propagation length required for phase-matched buildup to optimal conversion efficiency is 10's of cm.* All these parameters are quite different from past implementations of HHG, and mean that propagation issues are both critically important, and fall within a parameter regime that is similar to DE applications. This recent data combined with simulations from Alex Gaeta's group suggest that filamentation is important and can be har g process to create self-guided, bright, keV high-harmonics. It is i n Ti:sapphire lasers at a wavelength of 800nm are used to n waveguides, filamentation happens at lower pressures (≈ 5 r phase matching in Ar (≈ 30-60 torr to generate the brightest t photon energies around the 60 eV limit when using 800 nm s being submitted reporting these findings.

In other work in collaboration with Agnieszka Becker, we are using the velocity map imaging (VMI) techniques to image electrons after strong field ionization and rescattering from atoms and molecules in laser fields of different wavelengths (from 266nm to 4μm). We observe very distinct angular-dependent ionization for different wavelengths and laser intensities. Since the ionization and rescattering of electrons from molecules is sensitive to orientation, we first impulsively align the molecules. We demonstrate a high degree of control over electron trajectories in the vicinity of the Coulomb potential of the parent ion. The interference between the directly ionized and rescattered electrons strongly depends on the localization of the electron wavefunction in the vicinity of the parent ion at the instant of rescattering. The 2D interference pattern encodes attosecond electron dynamics, as well as information about the size of the returning electron wave packet. Also, the interference between the direct and returning electrons provides a direct measurement of the electron-ion differential cross section, which is found to vary significantly for different atomic and molecular targets. A paper is being submitted reporting these findings.

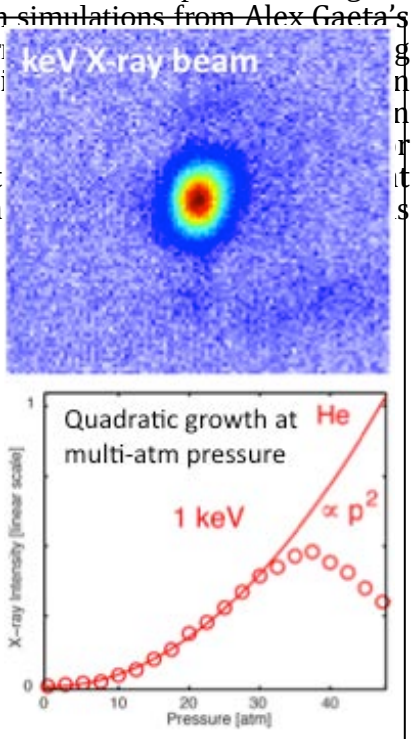

Fig. 1. (left) Spatial profile of the phase-matched, coherent, high harmonic X-ray beam around 1keV. The beam quality is excellent, with no evidence of distortion even at multi-atm pressures, leading to the question of how important filamentation effects are in stabilizing the phase matching process. (right) Quadratic growth of the soft x-ray HHG signal at 1 keV at pressures of the tens of atms.

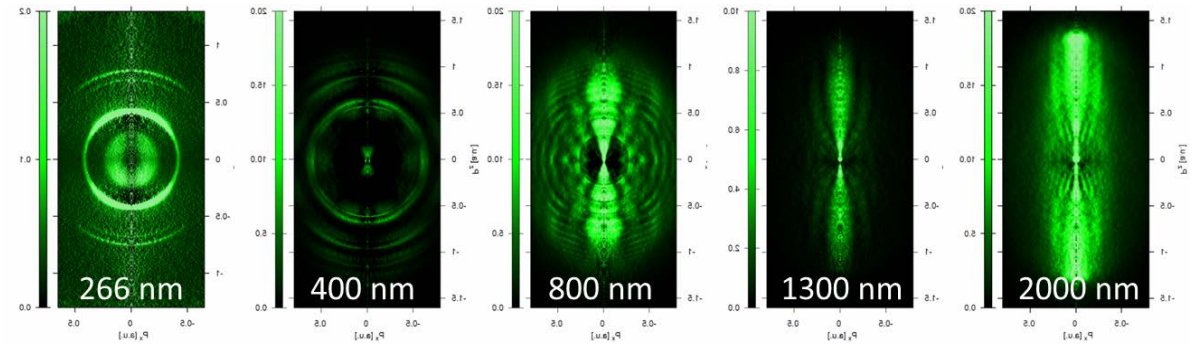

Fig. 2. Experimental photoelectron spectra collected with our VMI spectrometer, showing different structure at various wavelengths with the same laser intensity (~$1x10^{14}$ W/cm^2). The structure encodes information about ionization dynamics, electron wavepacket propagation dynamics, the structure of the parent ion, and graphically shows the transition from a multiphoton to a tunnel regime with increasing laser wavelength.

[1] M. C. Chen, *et al.*, "Bright, Coherent, Ultrafast Soft X-Ray Harmonics Spanning the Water Window from a Tabletop Light Source," *Physical Review Letters,* vol. 105, p. 173901, 2010.
[2] T. Popmintchev, *et al.*, "The Attosecond Nonlinear Optics of Bright Coherent X-Ray Generation", Nature Photonics," *Nature Photonics,* vol. 4, p. 822, 2010.
[3] T. Popmintchev, *et al.*, "Bright Coherent Attosecond-to-Zeptosecond Kiloelectronvolt X-ray Supercontinua," *CLEO Postdeadline Paper,* vol. PDPC12, 2011.
[4] B. Shim, *et al.*, "Filamentation in air with ultrashort mid-infrared pulses," *Optics Express,* vol. 19, pp. 9118-9126, 2011.
[5] N. L. Wagner, *et al.*, "Self-compression of ultrashort pulses through ionization-induced spatiotemporal reshaping," *Physical Review Letters,* vol. 93, p. 173902, Oct 22 2004.
[6] X. S. Zhang, *et al.*, "Phase matching, quasi-phase matching, and pulse compression in a single waveguide for enhanced high-harmonic generation," *Optics Letters,* vol. 30, pp. 1971-1973, Aug 1 2005.
[7] P. Arpin, *et al.*, "Enhanced high harmonic generation from multiply-ionized argon above 500 eV through laser pulse self compression," *Physical Review Letters,* vol. 103, p. 143901, 2009.
[8] A. Rundquist, *et al.*, "Phase-matched Generation of Coherent Soft X-rays," *Science,* vol. 280, pp. 1412-1415, 1998.

Papers in preparation as a result of MURI

1. "Bright Coherent Attosecond Kiloelectronvolt X-ray Supercontinua", T. Popmintchev, M.C. Chen, D. Popmintchev, S. Ališauskas, G. Andriukaitis, T. Balčiunas, A. Pugzlys, A. Baltuška, M.M. Murnane, H.C. Kapteyn (in preparation, 2011).
2. "Holography using spherical and plane electron waves", (in preparation, 2011).

MURI Annual Report

PI: Demetrios Christodoulides
MURI AWARD: AFOSR FA 9550-10-1-0561
School of Optics/CREOL
University of Central Florida
Period: Sept 30, 2010 to Sept 29, 2011
Date: September 22, 2011

Scientific Progress and accomplishments

During this period we made progress on several fronts. More specifically we made contributions in the understanding of beam dynamics associated with diffraction-free beams and other families of conical waves. The prospect of utilizing such beams and bullets under nonlinear conditions for optical filamentation studies is currently assessed.

Autofocusing optical beams:

1. **Theory of autofocusing optical beams**

In a recent paper (OL 35, 4045 (2010)) we introduced the possibility for a new family of radially symmetric (cylindrical and spherical) waves with a certain desired characteristic: their maximum intensity remains almost constant during propagation, while close to a particular focal point, they suddenly autofocus and, as a result, their peak intensity can increase by orders of magnitude. In two dimensions, we presented two different classes of such waves, which are based on a radial Airy profile and a superposition of two-dimensional Airy wave packets. In three dimensions, the spatiotemporal problem was exactly solved in the region of anomalous dispersion. In this latter case, even higher intensity contrasts can be expected. Figure 1demonstrates this behavior in a three-dimensional setting. It is important to point out that the general concept of autofocusing presented here is more general and, in principle, can be extended to other wave functions beyond Airy. However, the curved non-diffracting dynamics of Airy beams has several advantages, including enhanced autofocusing contrast and abruptness, especially in the case of long focal lengths. Other families of beams might also exist, exhibiting abrupt autofocusing properties.

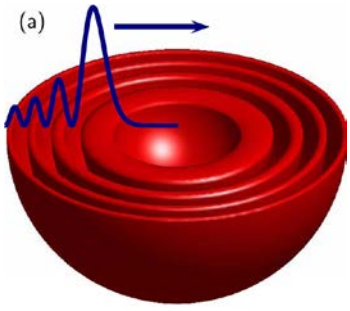

Figure 1. Three-dimensional spatio-temporal autofocusing dynamics in dispersive media.

2. **Observation of abruptly autofocusing waves:**

Quite recently we presented the first experimental observation of optical autofocusing behavior (Optics Letters vol. 36, 1842, 2011). This work was carried out in close collaboration with Tzortzakis's group from FORTH Crete-Greece. The experimental realization of abruptly autofocusing waves was performed using a radially symmetric Airy intensity distribution. We demonstrated that these waves can autofocus, with the

intensity maxima following a parabolic trajectory. The intensity contrast achieved was clearly much higher than that of a typical Gaussian beam, making these waves interesting candidates for a variety of applications, ranging from nonlinear filamentation experiments to laser surgery. The experiments were performed using 1 mJ, 35 fs laser pulses at 800 nm, with a Gaussian in space and time distribution, produced by a 50 Hz, Ti: sapphire laser system. The intensity contrast, defined as the ratio of the peak intensity along the propagation to the peak intensity at the Fourier plane is shown in Fig. 2. As expected, the intensity peak follows a curved trajectory as the wave propagates toward the focus. Furthermore, the intensity contrast is abruptly increased at the focus-as expected from theory. The rate that this is accomplished greatly exceeds that expected from a Gaussian beam-see Fig. 3. It is interesting to note that the observed autofocusing is an inherent property of the wave-i.e., it is not caused by any nonlinear effect such as self-focusing. The intensity contrast of the autofocusing wave was very low before the focus, while it increased up to ~195 times at the focus. The theoretical predictions nicely agreed with the experimental points, confirming that the radius contracts in a quadratic fashion.

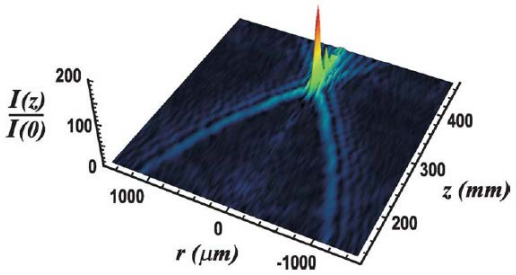

Figure 2. Autofocusing behavior of a radially symmetric Airy beam as a function of distance.

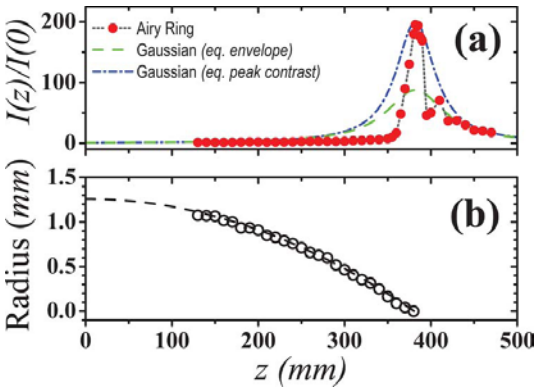

Figure 3. Rapid increase of intensity because of auto-focusing (red). The Gaussian response is less drastic.

Finally, in addition to their spatial profile, the temporal profile of these beams can be engineered to drastically enhance the intensity contrast at the focus.

3. **Pre-engineered abruptly autofocusing beams**

In a recent study (Optics Letters vol. 36, 1890-1892 (2011)) we have shown that the autofocusing dynamics of a certain class of waves can be very effectively pre-engineered. These are circularly symmetric wavefronts whose input amplitude develops outward of a dark disk and oscillates radially with a sublinear chirp signal. During propagation, these wavefronts form inward-bending caustic surfaces of revolution with an acceleration that is directly related to their chirp rate-see Fig.4. In this regard we have extended the family of circular Airy beams, the rays of which are known to form paraboloids- as a result of the quadratic inward radial shift of the Airy rings. Of course this new flexibility comes at the cost of losing the unique diffraction-resisting properties of the Airy waveform, which is, however, here traded for greater transverse accelerations, enhanced focusing abruptness,

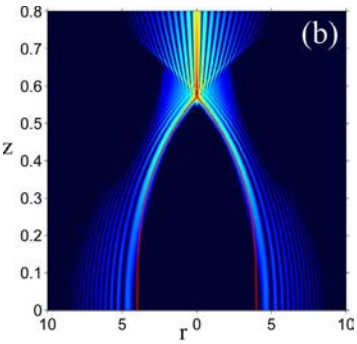

Figure 4. Abrupt autofocusing along a cubic optical caustic.

and larger intensity contrasts. By virtue of the chirped radial oscillations of their input amplitude, these new families of waves can abruptly focus their power after following caustic surfaces of revolution of any desired order. There are two degrees of freedom in pre-engineering this auto-focusing process: the radial chirp rate, which determines the shape of the caustic, and the envelope profile, which can be designed to increase the contrast and tailor the shape of the focusing spot. Beams with higher chirp rates are in general appropriate for enhanced abruptness and greater intensity contrasts, however, at shorter focal distances.

4. **Fourier-space generation of abruptly autofocusing beams and optical bottle beams**

Lately, a highly accurate closed-form expression has been reported for the Fourier transform of an autofocusing beam. Through asymptotic analysis, we have shown that the spectrum behaves like a first-order Bessel function that oscillates with a quadratic chirp rate due to an additional cubic phase term. The spectrum amplitude was apodized in a Gaussian fashion. The derived spatial spectrum can be used to produce wavefronts that evolve into autofocusing beams with desired characteristics after being Fourier-transformed by a thin lens. We showed that, depending on the relation between the chirp rate and the lens' focal distance, such a beam can have one or two foci. In the second case, the two foci are symmetric with respect to the lens' focal plane, thus creating an elegant optical bottle with paraboloid multilayer boundaries and two closed ends. The formation of such an optical bottle beam is shown in Fig. 5. Experimentally, we successfully demonstrated such an optical bottle using this class of waves. Our findings also explain the morphing of autofocusing beams to expanding Bessel-like beams in the Fraunhofer region. Optical bottle beams, can be very useful in several settings like particle guiding and trapping.

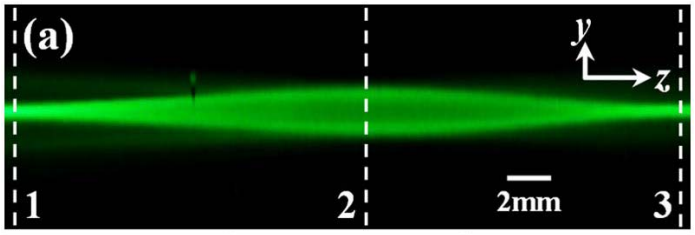

Figure 5. Experimental demonstration of an optical bottle beam-forming using autofocusing.

<u>Self-accelerating Airy-like solitons:</u>

We have also studied shape-preserving accelerating beams in nonlinear media that propagate along parabolic trajectories and derived their existence curve (Physical Review Letters vol. 106, pp. 213903 (2011)). We have considered other self-accelerating beams, especially the asynchronous solutions for quadratic nonlinearities. We took into account finite aperture effects and showed how accelerating beams can be implemented experimentally. Applications are expected for high intensity beams, where the acceleration can be changed by varying the intensity, because of self-focusing nonlinearities. Other possibilities may include nonlinear accelerating beams in media displaying thermophoresis or photophoresis, where light controls the local density of particles within the liquid or gas.

Scientific personnel: Mr. Matthew Mills (Ph.D. student)
Mr. Mohammad Ali Miri (Ph.D. student)

Technical Interactions: In early June 2011, Dr. Tobias Graf from Dr. Moloney's group has visited CREOL. During his visit, he interacted with the graduate students here concerning nonlinear Bessel beam propagation and optical bullets in dispersive systems. A paper along these lines is now in preparation.

Report of inventions: NA
Technology transfer: NA

Papers published during this period relevant to MURI activities

1. P. Zhang, J. Prakash, Z. Zhang, M. Mills, N. Efremidis, D. Christodoulides, and Z. Chen, "Trapping and guiding micro-particles with morphing auto-focusing Airy beams", Optics Letters, vol. 36, pp. 2883 (2011).

2. N. K. Efremidis and D. N. Christodoulides, "Abruptly autofocusing waves," Optics Letters vol. 35, 4045-4047 (2010).

3. D. G. Papazoglou, N. K. Efremidis, D. N. Christodoulides, and S. Tzortzakis, "Observation of abruptly autofocusing waves," Optics Letters vol. 36, 1842-1844 (2011).

4. Chremmos I., N. K. Efremidis, and D. N. Christodoulides, "Pre-engineered abruptly autofocusing beams," Optics Letters vol. 36, 1890-1892 (2011).

5. Chremmos I., P. Zhang, J. Prakash, N. Efremidis, D. N. Christodoulides, and Z. Chen, "Fourier-space generation of abruptly autofocusing beams and optical bottle beams", Optics Letters, vol. 36, pp. 3675 (2011).

6. Chong, W. H. Renninger, D. N. Christodoulides, and F. W. Wise, "Versatile Airy-Bessel light bullets", Optics and Photonics News, December issue, Optics in 2010, pp. 52 (2010).

7. P. Zhang, Z. Zhang, J. Prakash, S. Huang, D. Hernandez, M. Salazar, D. N. Christodoulides, and Z. Chen, "Trapping and transporting aerosols with a single optical bottle beam generated by Moiré techniques", Optics Letters, vol. 36, pp. 1491 (2011).

8. Kaminer I., M. Segev, and D. N. Christodoulides, "Self-Accelerating Self-Trapped Optical Beams", Physical Review Letters vol. 106, pp. 213903 (2011).

Papers submitted/in preparation for publication (relevant to MURI activities)

Kaminer I., Yaakov Lumer, and M. Segev, and D. Christodoulides, "Causality Effects on Accelerating Light Pulses", submitted to Optics Express.

M. Mills, G. Siviloglou, D. Christodoulides, T. Graf, and J. Moloney, "Optical bullets with Hydrogen-like symmetries", to be submitted, Physical Review A.

Book contributions/Articles

Salandrino A. and D. Christodoulides, "Airy plasmons defeat diffraction on the surface", Physics 4, 69 (2011) – Published September 6, 2011.

Colloquia

D. N. Christodoulides, "Optical Airy beams and bullets", Dept. of Mathematics, US Naval Academy, Annapolis, October 14, 2010.

D. Christodoulides, "Optical Airy beams and bullets", Physics Department. U. of Miami, February 16, 2011.

D. Christodoulides, "Optical Airy beams and bullets", Optical Sciences Center, U. of Arizona, March 24, 2011.

Conference presentations (relevant to MURI activities)

P. Zhang, Z. Zhang, J. Prakash, S. Huang, D. Christodoulides, Z. Chen; "Trapping and manipulating aerosols with optical bottle beams generated by Moiré technique,", paper QWI6, CLEO 2011, Baltimore, Maryland, May 1-6, 2011.

N. K. Efremidis, D. Christodoulides, I. Chremmos, Z. Chen; "Abruptly autofocusing waves", paper QThS1, CLEO 2011, Baltimore, Maryland, May 1-6, 2011.

Ido Kaminer, M. Segev, D. Christodoulides, "Self-Accelerating Self-trapped Beams", paper CThFF5, CLEO 2011, Baltimore, Maryland, May 1-6, 2011.

Peng Zhang, J. Prakash, Z. Zhang, Y. Hu, N. Efremidis, V. Kajorndejnukul, D. Christodoulides, Zhigang Chen, "Observation of auto-focusing radially symmetric Airy beams", paper QThS7, CLEO 2011, Baltimore, Maryland, May 1-6, 2011.

Ido Kaminer, M. Segev, D. Christodoulides, "Can Quadratic Solitons Self-Accelerate", paper QFF7, CLEO 2011, Baltimore, Maryland, May 1-6, 2011.

D. Christodoulides, "Airy Beams and Bullets", invited talk, Asymptotics, phases and chaos, Optical and Quantum Conference in Honor of Michael Berry's 70th Birthday, Universidad Nacional Autónoma de México, Cuernavaca, México, September 7th to 9th, 2011.

MURI Annual Technical Report, Temple University

1. Personnel

Professor Robert J. Levis
Professor Dmitri Romanov
Mr. Johanan Odhner
Ms Erin McCole
Ms. Maryam Tarazkar

Publications:

1. Post-ionization medium evolution in a laser filament: uniquely non-plasma response, Romanov, D.A, Levis R.J submitted to PRL
2. Theoretical study of the polarizability and second order hyperpolarizability for N_2 and N_2+, Tarazkaris M, Romanov D.A, Levis RJ. in preparation for J. Phys. Chem. A
3. Direct Temporal Phase and Amplitude Characterization of Femtosecond Laser Pulses Undergoing Filamentation in Air, Odhner, J.H, Levis R.J, inpreparation for PRL

Summary of Experimental Investigations:

Measurements of filamentation dynamics in the filament are a key part of supporting the theoretical aspects of this MURI effort. Our efforts have focused on characterization of the spectral phase and amplitude as a function of propagation distance in the filament to understand the role of the nonlinear processes governing filamentary dynamics in ultrashort pulses. Processes contributing to these dynamics include Kerr lensing and plasma formation. Underway are experiments aimed at determining the importance of reported nonlinear effects such as the higher-order Kerr effects.

We have measured pulses undergoing filamentation using transient-grating cross-correlation frequency-resolved optical gating (TG-XFROG), wherein two weak pulses create a transient refractive index grating in the filament propagation medium and a portion of the filament pulse undergoes diffraction from this grating. The time-resolved signal is measured and the pulse spectral and temporal phase and amplitude are retrieved using an iterative algorithm. Measurement of a 1.5 mJ, 50 fs pulse undergoing filamentation 2.5 m after being focused with a 2-m lens is shown in Figure 1. The measured result is in excellent agreement with previously reported post-filament pulse measurements. To garner insight into the role of the contributing nonlinearities, we did a power study of the filament pulse shape in the filament, shown in Figure 2. In the context of previous work performed in this group [Odhner:2010], the measurements suggest that plasma generation dominates at lower intensities, causing on-axis pulse splitting that is sustained along the length of the filament. At higher input power, the trailing part of the pulse has sufficiently high power that after the main plasma generation event the pulse re-focus at a later time, leading to effective temporal shortening of the pulse on axis to < 7fs.

Summary of Theoretical Investigations:

i. The role of transient resonance on the way to plasma equilibrium.

The issue of the role that ionization of the medium plays in laser filamentation is currently the center of growing controversy. We developed a conceptual model for a fundamental difference between the nascent state of ionization in the filament-bearing medium and a low-density plasma. The characteristic distances between atoms/molecules in a gas at atmospheric pressure is about ~30 Å. At the same time, at the typical ion density in a filament $n \sim 10^{15}$ cm^{-3}, the average distance between ions is ~ 1000 Å. At the velocity of ~10^7 cm/s, the released electron covers only ~20 Å during a ~ 20 fs laser pulse. This means that during filamentary propagation, the ionization process does not produce a uniform plasma by the end of the laser pulse. Shortly after ionization, rather, the isolated and well-separated ions are each surrounded by an expanding electron cloud. This cloud is initially formed by the wavepacket emerging from the ionization process, and the spatial extent of the wave packet can be estimated ~ 2.5 Å. The essence of the medium response is conceptually unaltered by the details of the electron cloud expansion, which we therefore considered under very general (and simplifying) assumptions. A simple analytical model describes oscillations of these virtually isolated and expanding electron clouds, forced by the laser field. The model predicts considerable enhancement of these oscillations caused by transient resonance with the laser carrier frequency, as shown in Figure 3. As a result, the electromagnetic response of the medium differs significantly from the familiar plasma picture. The obtained results impact the currently accepted picture of filament formation dynamics and call for modifications in existing theoretical models.

ii. A Theoretical study of polarizability and second order hyperpolarizability for N_2 and N_2 cation.

We have investigated the nonlinear polarizability of the constituents of air, namely N_2 and O_2. The process of filamentation is initiated through the intensity-dependent index of refraction that accompanies the passage of strong-field laser radiation through a medium. Ongoing attempts at controlling filamentation require better understanding of the delicate balance of the Kerr focusing and plasma defocusing. These developments have been the main source of our motivation to investigate closely how the nonlinear optical behavior of air-constituent molecules is modified upon ionization. Even for neutral molecules, their polarizability and hyperpolarizability are notoriously difficult to determine experimentally. For corresponding molecular ions, there are no pertinent experimental data whatsoever. Thus, theoretical calculations based on appropriate quantum chemistry methods provide virtually the only route toward determining these characteristics.

We set out on a systematic program of establishing theoretical values for ionic polarizabilities and hyperpolarizabilities for the major air constituents and various admixture molecules that may be utilized towards filament control. We intend to use the existing data on neutral nitrogen to benchmark these calculations, and we pay special attention to adopting the same procedural details for neutral molecules and their cations.

Our preliminary results for nitrogen ion show two major trends. First, upon ionization, the anisotropy of the polarizability reverses its sign. Second, the value of ionic hyperpolarizability is more than an order of magnitude higher than that for neutral. Should these trends be confirmed and extended to oxygen, significant corrections would be in order for correct description of the filament.

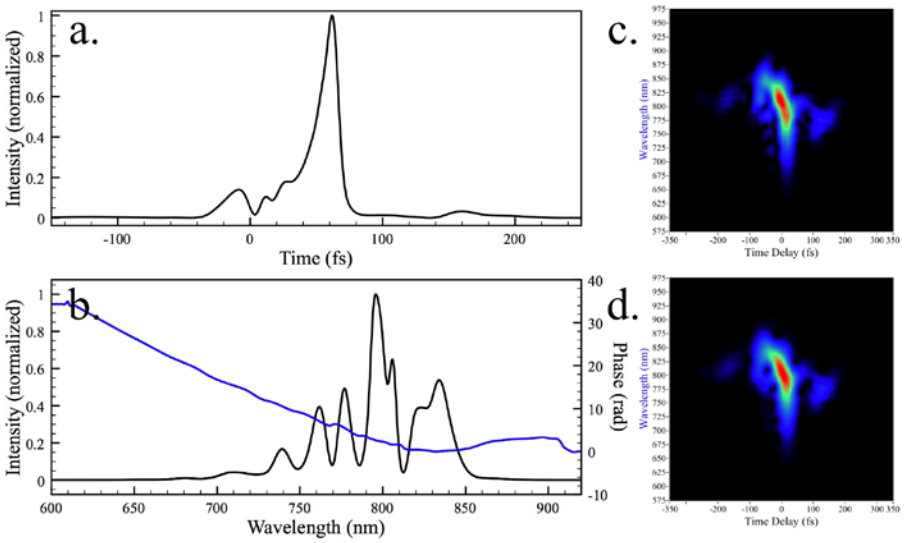

Figure 1. Full retrieval of a pulse measured while undergoing filamentation in air at three times the critical power for self-focusing. Shown are: a) the temporal intensity of the measured pulse, b) spectral intensity and phase corresponding to the measurement in (a), and the measured (c) and retrieved (d) spectrograms corresponding to (a) and (b).

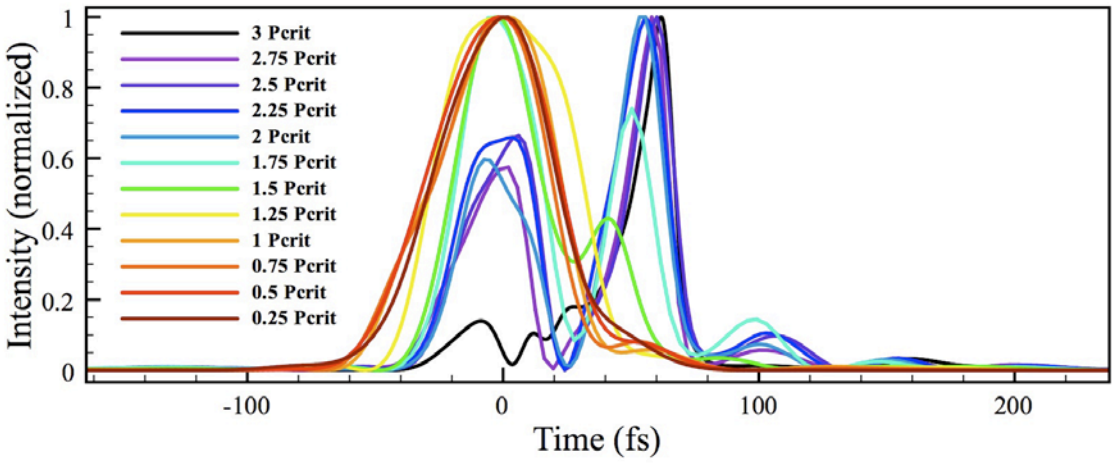

Figure 2. Temporal profile of the filament pulse as a function of input power. As the power is increased, pulse splitting occurs and isolation of the trailing pulse is observed at the highest input power used here.

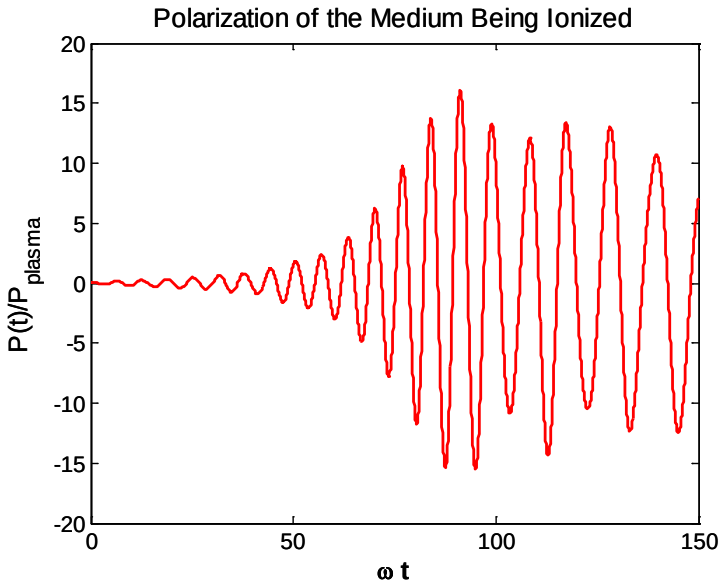

Figure 3. The cumulative polarization response of a medium that is being tenuously ionized by a laser pulse with rectangular envelope. The observed drastic enhancement of fhe oscillation amplitude is due to passage through the transient resonance.

Colorado School of Mines

Spatio-temporal characterization and control of ultrafast nonlinear beam dynamics

Charles G. Durfee and Jeff A. Squier *coPIs*
Department of Physics, Colorado School of Mines

Student supported: Amanda Meier (2nd year PhD). Ms Meier attended the student workshop in March 2011. She made a second trip in August 2011 to Tucson and spent a day with Miroslav Kolesik learn to run the UA propagation code.

At CSM we are using techniques to characterize the spatio-temporal properties of beams that are undergoing nonlinear propagation in solid-density and gas-density media. We are also working with a novel technique to focus spatially-chirped beams to achieve strong localization in intensity. Our aims are to:

- apply spatially- and spectrally-resolved interfereometry (SSRI) to measure the evolution of these complex fields to better understand the nonlinear coupling of the medium and the propagating field
- characterize the nonlinear response of the medium through the characterization of the fields after propagating through thin samples
- explore the control of the nonlinear beam propagation through the manipulation of the input spectral distribution (spatial chirp)

Year 1 progress

SSRI system: The SSRI measurement depends on linear interferometry between a pulse that is well-characterized spatially and spectrally and the test beam. In this reporting period, as part of the training of new students working in this area, we worked to improve the quality and characterization of the SSRI reference beam.

- Along with the short-pulse output, many laser systems have an appreciable amount of the output energy in a long-duration pedestal (amplified spontaneous emission, ASE). Since the SSRI measurement is linear, interference can occur between the long pulses of light, in addition to the desired interaction between the short pulses. This additional interference pattern can adversely affect the measured interference pattern. We developed a way to use interferometry to measure the energy fraction in the ASE: in one arm of the interferometer, the beam undergoes a non-linear cross-polarized wave (XPW) conversion process in BaF2. This third-order process acts as a time filter that strongly filters out any long-pulse light. When this pulse interferes with the beam from the amplifier, the two coherent short pulses will interfere, leaving a background that results from the ASE. This measurement is capable of measuring energy fractions below a few percent.
- To characterize the light in the filament that has a strongly broadened spectrum, the reference beam must have an equal or greater bandwidth, preferably with a smooth spectral profile. We have set up an optical system that first broadens the pulse bandwidth in a gas-filled hollow capillary, which results in a broad spectrum that is strongly modulated, but with a smooth spatial profile. The output spectrum is compressed with a pair of chirped mirrors, then focused into a thin (0.5mm) BaF2 crystal for XPW conversion. The time-filtering of the XPW process eliminates the temporal side-lobes, thereby broadening and smoothing the output spectrum (see Fig 1)

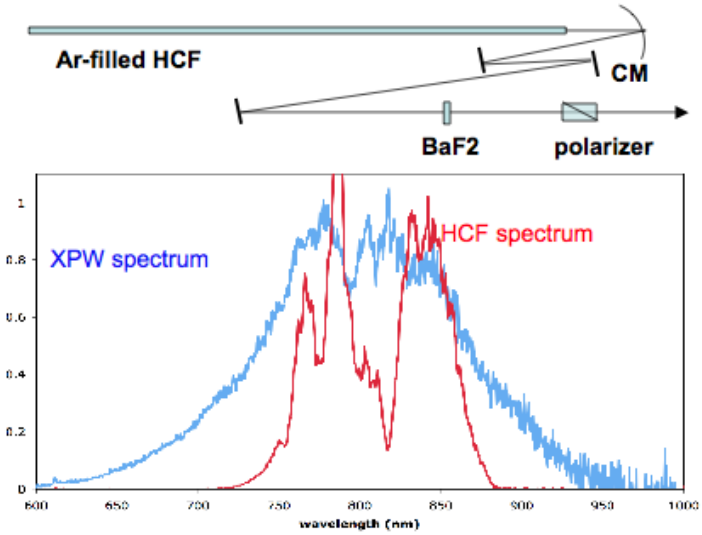

Figure 1. Schematic of layout to produce a smooth beam that is time-filtered with cross-polarized wave generation (XPW).

Spatial-chirp focusing: A beam with lateral spatial chirp has a linear variation of the frequency across the beam. When this beam is focused with a curved mirror, the intensity is suppressed away from the focus because of the spread in frequency components. At CSM we have used this technique successfully for micromachining: filamentation is averted along the way to the high intensity focus, allowing for waveguide writing and machining on the backside of transparent samples. As part of this MURI, we are investigating the intensity localization control this method offers. We have developed a general analytical method for propagating spatially-chirped Gaussian beams and to calculate the spectral and temporal characteristics throughout the focus. Each frequency component is treated as its own Gaussian beamlet, which is propagated through the optical system. Figure 2 illustrates how the intensity localization works: the black curve represents intensity I(z) through the focus for a single frequency beamlet. Simply spreading the beam across one dimension tends to localize the intensity (red), but the fact that the local bandwidth is reduced away from the focus leads to a further localization (green). Still more localization (blue) results from a chirping effect: the shape of the tilted, curved wavefronts introduces a geometric dispersion away from the focus. These analytic calculations provide a framework for the design of We have set up an optical system to do space-time focusing of several mJ of ultrashort pulses in air, and will be using this arrangement to investigate nonlinear propagation and THz generation.

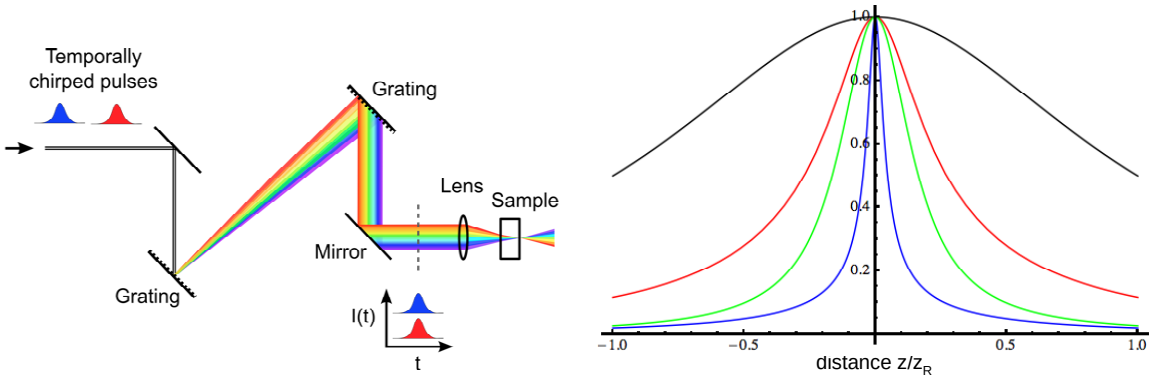

Figure 2. Left: experimental schematic for generating a spatially-chirped focus. Right: Intensity through the focus, with distance normalized to the Rayleigh range of an individual ω beamlet (black). Red: I(z) accounts for the additional increase in the beam area away from the focus; green: I(z) accounts for the additional increase in the transform limited pulse duration; blue: accounts for the geometric spectral chirp.

Invited talk – Ultrafast Optics 2011, Monterey, CA “Femtosecond micromachining using simultaneous spatio-temporal focusing,” Jeff A. Squier, Dawn N. Vitek, Erica Block, Michael Young, Charles G. Durfee

Contributed talk/proceedings:

"Measurement of Energy Contrast of Amplified Ultrashort Pulses using Cross Polarized Wave Generation and Spectral Interferometry," M. Iliev, A. K. Meier, D. E. Adams, J. A. Squier, and C. G. Durfee, in CLEO:2011 - Laser Applications to Photonic Applications, OSA Technical Digest (CD) (Optical Society of America, 2011), paper CTuO2.

MURI technical report

Cornell University, Alexander Gaeta

Publications:

"Loss-of-Phase with Collapsing Beams," B. Shim, S. E. Schrauth, and A. L. Gaeta, M. Klein, and G. Fibich, submitted to Phys. Rev. Lett. (2011).

Invited Talks

1. "Loss-of-phase with high-power collapsing beams," Ultrafast Optics 2011, Monterey, CA, September 28, 2011.
2. "Loss-of-phase with high-power collapsing beams," International Laser Physics Workshop, Sarajevo, Bosnia and Herzegovina, July 13, 2011.

1. Loss of phase with collapsing beams

We have investigated the loss-of-phase of high-power collapsing beams in a Kerr-medium. Fibich and Klein [1] theoretically predicted that when a high-power beam undergoes self-focusing and beam collapse, the beam acquires a large cumulative nonlinear phase shift after collapse and this accumulated phase is highly sensitive to small fluctuations of the laser power. As a result, the phase of a laser pulse after collapse will be stochastic and we call this effect "loss-of-phase". First we experimentally confirm this prediction by directly measuring the phase of a collapsing beam in a water cell with the Mach-Zehnder interferometry technique. Figure

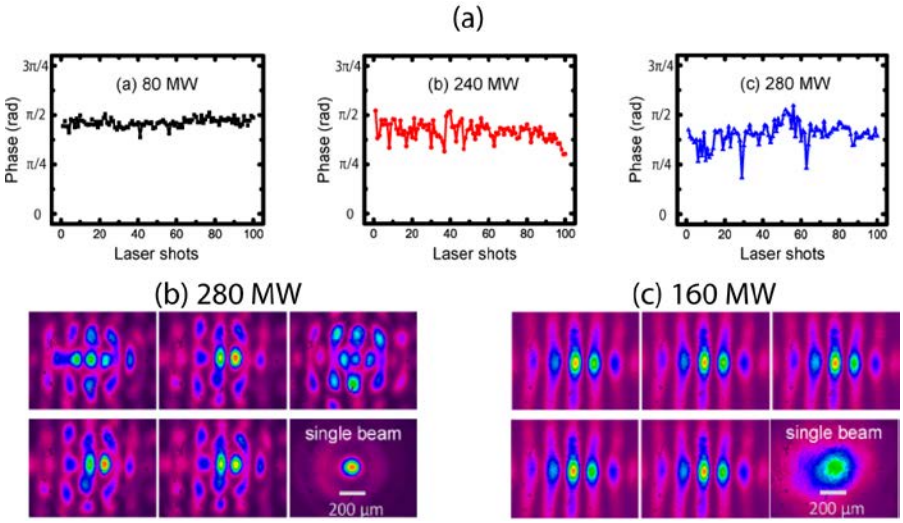

Fig. 1. (a) Measured phase of high-power beams in a Kerr medium (24-cm water cell) for different input beam powers. When the beam undergoes collapse at 240 and 280 MW powers, we observe shot-to-shot fluctuations in the extracted phase, which is due to the loss-of-phase. (b) Two crossing beam profiles at the output of the 24-cm water cell for high-power collapsing beams (P = 280 MW for each beam). There are significant fluctuations in the output intensity profiles since the loss-of phase effect is large for collapsing beams. (c) Two crossing beam profiles at the output of the 24-cm water cell for low-power, non-collapsing beams (P = 160 MW for each beam). There are minimal fluctuations in the output intensity profiles.

1(a) shows the experimentally extracted phase of 100 laser shots for different powers. When the input beam power is 80 MW, the beam does not undergo collapse and phase fluctuations are minimal. However as the input beam power is increased such that the beam experiences collapse inside the water cell, phase fluctuations also increase due to the loss-of-phase effect.

Second, we demonstrate this loss-of phase effect by observing fluctuations in intensity profiles when two collapsing beams with the fixed initial phase interact near the collapse point in small, crossing angle geometry (0.2^o). When the input power of each beam is 280 MW, each beam undergoes collapse and evolves into a symmetric, Townes-like profile about 200-μm diameter [the last figure in Fig. 1(b)]. Although we expect two collapsing beams would demonstrate (partial) fusion via constructive field interference when we set the initial phase as zero, Fig. 1(b) clearly shows significant shot-to-shot fluctuations in the output intensity profiles due to loss of phase. As a comparison, for the 160 MW input power, each beam does not collapse inside the water cell [the last figure in Fig. 1(c)] and thus we observe minimal fluctuations as is shown Fig. 1(c). These results are highly relevant to understanding the turbulent behavior that can occur with beams containing multiple filaments and to the capability of controlling filament interactions [2].

[1] G. Fibich and M. Klein, Nonlinearity **24,** 2003 (2011) .
[2] M. Mlejnek *et al*., Phys. Rev. Lett. **83**, 2938 (1999); L. Berge *et al*., Phys. Rev. Lett. **92**, 225002 (2004).

2. Self-focusing induced enhancement of high-order harmonic generation

Kapteyn and Murnane's (KM) group at University of Colorado at Boulder and JILA experimentally observed strong enhancement of high-order harmonic generation (HHG) and spatially bright and narrow soft x-ray beam profiles with mid-infrared ultrashort pulses when they increased the Ar pressure inside of capillary. The pressure used for this bright soft x-ray

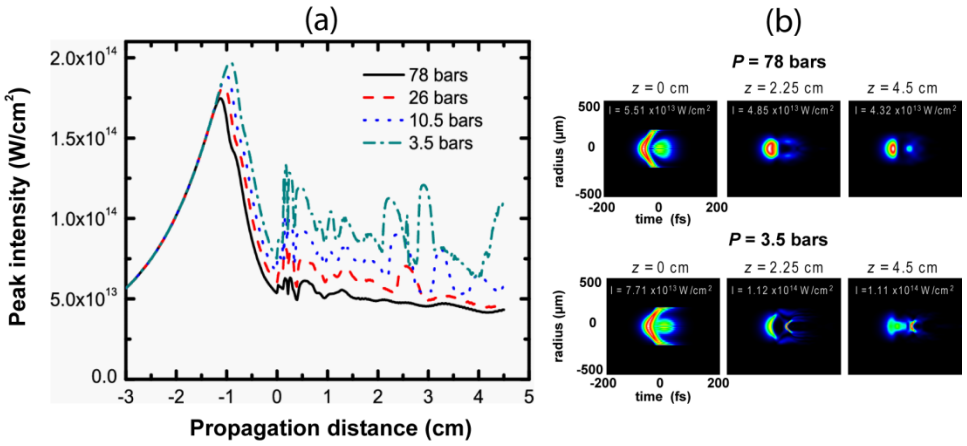

Fig. 2. (a) Peak intensity vs. laser propagation distance for different Ar pressures. Here z = 0 cm is the capillary input and z = 4.5 cm is the capillary output. As the pressure increases, the peak intensity becomes more stable due to self-focusing and filamentation effect. (b) Examples of spato-temporal profiles at three different locations for two different pressures 78 and 3.5 bars.

generation is much higher than the conventional phase matching pressure, and thus self-focusing becomes important since the critical power for self-focusing is inversely proportional to the gas pressure. In collaboration with KM group and M. Kolesik and J. Moloney of University of Arizona, we have performed simulations of laser propagation in capillary using the nonlinear envelope equation [1] and observed the stable propagation regime for high pressure Ar gas via self-focusing and potential filament formation. As shown in Fig. 2(a), the peak intensity of the driving laser (3.9-μm wavelength) inside capillary remains almost constant at higher pressures (*e.g.* 78 bars) and the spatio-temporal profiles show the solitary wave behavior, which contribute to enhancement of HHG. As a comparison, the peak intensity at lower pressures (*e.g.* 3.5 bars) shows the oscillatory behavior and the spatio-temporal profiles are much more complicated. Currently, we are incorporating the phase matching calculation in our code and also investigating the laser propagation and its effect on HHG using different gases such as He and Ne.

[1] A. L. Gaeta, Phys. Rev. Lett. **84**, 3582 (2000).